Flow-through electrodes enable order of magnitude higher partial current densities in aqueous CO_2 electrolysis

Ligthart, Nathalie E.G.; Khan, Mohammed A.; Padding, Johan T.; Vermaas, David A.

DOI
10.1016/j.jcou.2025.103248

Publication date
2025

Document Version
Final published version

Published in
Journal of CO2 Utilization

Journal of CO2 Utilization 102 (2025) 103248

Contents lists available at ScienceDirect

Journal of CO2 Utilization

journal homepage: www.elsevier.com/locate/jcou

Flow-through electrodes enable order of magnitude higher partial current densities in aqueous CO_2 electrolysis

Nathalie E.G. Ligthart [a], Mohammed A. Khan [a], Johan T. Padding [b], David A. Vermaas [a,*,1]

[a] Department of Chemical Engineering, Delft University of Technology, Van der Maasweg 9, Delft 2629HZ, the Netherlands
[b] Department of Process and Energy, Delft University of Technology, Leeghwaterstraat 39, Delft 2628CB, the Netherlands

ARTICLE INFO

Keywords:
CO_2 reduction
Suspension electrode
Flow-through electrode
Electrolysis
Surfactants
Flow chemistry
Mass transport

ABSTRACT

Electrochemical conversion of CO_2 to hydrocarbons is limited by the low solubility and slow transport of CO_2 in aqueous systems. We demonstrate that we can reach partial current densities for CO_2-to-CO of 40 mA/cm^2 in fully aqueous systems, without the use of gas diffusion electrodes. We alleviate the mass transfer limitation by combining a suspension of catalytically active silver nanoparticles (Ag NPs) with a flow-through current collector. This extends the reactive area into the electrolyzer channel and improves the accessibility of dissolved CO_2 in a larger volume of electrolyte. The flow-through electrode system also outperforms a fully suspended electrode (based on carbon black particles), due to enhanced electric conductivity and smaller carbon area to minimize parasitic side-reactions. Additionally, we show that the distribution of the Ag NPs is pivotal for high CO_2 conversion rates, demonstrated by the highest CO current density obtained when a suspension of Ag NPs and SDS as surfactant is flowing through the 3D electrodes as pre-treatment. A stable CO current density can be sustained for more than 4 h. Although the conversion rate is still moderate compared to gas-fed CO_2 electrolzyers, the partial current density for flow-through electrodes is more than an order of magnitude larger than for planar flow systems. This work shows that CO_2 conversion in aqueous systems can be enhanced considerably by exploiting larger electrolyte volumes via smart electrode designs, such as a flow-through principle.

1. Introduction

The excessive CO_2 levels in our atmosphere are driving a global need to transition to fossil-free renewable energy, fuels, and materials. [1,2] Electrochemical CO_2 reduction is gaining attention as a clean route to convert CO_2 to basic carbon compounds (*e.g.* CO, ethylene, formic acid), and ultimately to synthetic hydrocarbons such as fuels, plastics, and green chemicals without consuming fossil fuels and releasing new CO_2. [3,4]

Despite the significant interest in electrochemical CO_2 reduction, the technology is challenging to commercialize. Early work on CO_2 reduction in water demonstrated good selectivity to CO and hydrocarbons using Ag or Cu catalysts. [5–7] However, H-cells with aqueous-based CO_2 reduction are typically limited to 2 mA/cm^2, due to low CO_2 solubility and slow mass transport, [8–10] while reaching current densities of at least 200 mA/cm^2 at high ($\geq$95 %) faradaic efficiency (FE) and low cell voltage ($\leq$3 V) [11] in scalable systems will be required to achieve economic viability. [12–14] Higher current densities are obtained in gas-fed CO_2 electrolysis configurations, using gas diffusion electrodes, that leverage improved mass transfer to achieve these targets at lab scales, but are suffering from complex water management [15–17], stability issues [18–21] and delicate heat management [22,23] in stacked and larger electrolyzers. At the same time, work on electrochemical H_2O_2 production [24], CO_2 reduction [25,26] and water electrolysis [27,28] has shown that (partial) current densities can be substantially increased by using 3D electrode structures. This raises the question whether mass transport can also be alleviated in a fully aqueous CO_2 electrolyzer system.

To address the mass transport limitations in fully aqueous systems, we studied volume-based aqueous systems, leveraging a larger electrolyte volume and making more reactant available, potentially leading to more robust and scalable systems. [26,29] Suspension electrodes, also known as semi-solid or flowable electrodes, enable the electric current to percolate deep into the electrolyzer channel and to reach otherwise inaccessible CO_2 molecules. [30] Although suspension electrodes have proven effective in various electrochemical applications (*e.g.* semi-solid

* Corresponding author.
E-mail address: D.A.Vermaas@tudelft.nl (D.A. Vermaas).
[1] orcid.org/0000–0002-4705–6453

https://doi.org/10.1016/j.jcou.2025.103248
Received 7 July 2025; Received in revised form 2 October 2025; Accepted 10 October 2025
Available online 17 October 2025

redox flow batteries [31,32], flow-electrode capacitive deionization [33,34], microbial fuel cells [35,36]), their application in CO_2 electrolysis introduces several challenges. A trade-off between conductivity and flowability results in a poor reaction distribution over the channel depth and creates dead zones where no reaction takes place. Additionally, the relatively large conductive area compared to the catalyst area can lead to increased competition with parasitic reactions, such as the hydrogen evolution reaction (HER). [37]

Further expanding the concept of volume-based electrodes, we introduce a flow-through current collector that effectively replaces the flowable conductive network with a static network. Incorporating a solid and continuous structure leads to higher electric conductivity than relying on intermittent particle-particle interactions [38,39]. Additionally, this strategy decreases the carbon surface area relative to the area active for CO_2 reduction, thereby minimizing side reactions. [40] Flow-through electrodes have already been applied successfully in other electrochemical applications such as redox flow batteries [41,42] and water electrolysis [28,43]. We expect that replacing the carbon particle network in a suspension by a static conductive network can lead to higher geometric current density and selectivity in aqueous CO_2 reduction as well.

Here, we demonstrate volume-based CO_2 reduction with suspensions of silver nanoparticles (Ag NPs) flowing through a 3D (foam) current collector. We compare the flow-through system with a conventional flow-by system and a carbon black (CB) suspension-based system. We reach geometric current densities for CO_2-to-CO conversion that are an order of magnitude higher than for flat electrodes and show that adding stabilizing agents improves the system further, demonstrating a viable pathway towards intensifying CO_2 reduction in aqueous flow systems.

2. Materials and methods

2.1. 3D electrode materials

All experiments were performed in a custom-made PMMA flow cell with 6 mm thick flow channels. A glassy carbon plate (Goodfellow) is embedded in the cathode endplate in the flow-by configuration. The flow-through configuration has a glassy carbon foam (Goodfellow RVC foam, 24 pores/cm, approximately 430 μm pore size, 6.35 mm thick) inserted in the flow channel on top of the glassy carbon plate (Fig. S1). We selected a foam that was slightly thicker than the flow channel (6.35 mm versus 6 mm channel thickness) to ensure good electrical connection between the glassy carbon foam and the plate. The glassy carbon plate was cleaned before each experiment by polishing and subsequent sonication in deionized (DI) water. The RVC foam was cleaned by sonicating and rinsing in DI water, after which the foam was dried in an oven at 150 °C.

2.2. Cell setup

The cell was assembled as shown schematically in Fig. S2a with a Selemion AMV (100 μm, AGC Engineering) membrane separating the catholyte and anolyte compartments. The membrane was soaked and stored in electrolyte before use. A Ti sheet with Ir-/Ru-oxide coating (Permascand) was used as anode, and a leak-free Ag/AgCl reference electrode (LF-1–45, Alvatek) was inserted into the anode compartment. The flow cell was connected to the electrolysis setup as shown in Fig. S2b.

2.3. Electrolyte preparation

An electrolyte of 0.5 M $KHCO_3$ (99 %, ThermoFisher Scientific) in deionized water was used for the catholyte and anolyte (both with a volume of 40 mL) unless otherwise noted. The catholyte suspensions were prepared by adding the desired type and amount of particles to the electrolyte and stirring for 10 min, followed by 15 min of sonication. Silver nanoparticles (Ag NPs, 99.9 %, ThermoFisher) were used as catalyst in suspension. For the surfactant-mediated solutions, we used sodium dodecyl sulfate (SDS) and Ag NPs capped by polyvinylpyrrolidone (Ag-PVP, 99.5 %, Merck). When SDS was used, the particles were added to the electrolyte, the suspension was stirred for 5 min and sonicated for 10 min before adding the required amount of SDS, followed by stirring and sonication for an additional 5 and 15 min, respectively. The types of particles, current collectors, and electrode configuration used in the different experiment types are listed in Table S1. The anolyte and catholyte were saturated with CO_2 by sparging 50 mL/min of CO_2, controlled by mass flow controllers (MFCs, Bronkhorst), for at least 30 min before each measurement. This was continued during the experiment to keep the electrolytes saturated and to flush the product gases to an inline gas chromatograph (CompactGC$^{4.0}$, Interscience) for analysis. The electrolytes were circulated at a flow rate of 80 mL/min (L/S Precision Pump System, Masterflex). A needle valve in the anolyte tubing was used to minimize the pressure difference between the two compartments and prevent membrane rupture.

2.4. CO_2 electrolysis methods

All electrochemical measurements were performed with an Ivium-Stat.h (±5 A/±10 V, Ivium), a XP20 (±20 A/±20 V, Ivium), or a PGSTAT302N (±2 A/±30 V, Autolab) potentiostat. Chronopotentiometry (CP) was performed at various geometrical current densities for 45 min each, during which the product gases were analyzed at time intervals of approximately 4 min with a CompactGC$^{4.0}$ (Interscience). A CP at 50 mA/cm^2 was always performed first, followed by CPs at 25–200 mA/cm^2 in a randomized order, and a second 50 mA/cm^2 at the end of the day for comparison. The electrolytes were resaturated with CO_2 for 30 min between each CP.

3. Results and discussion

We analyzed CO_2 electrolysis using a suspension of Ag NPs flowing through a carbon foam (Fig. 1b), a suspension of carbon black (CB) and Ag NPs flowing past a glassy carbon plate (Fig. 1c), and a silver plate (Fig. 1d). Employing a flow-through current collector with a flowing suspension of catalyst particles yields substantially higher CO current densities compared to the Ag/CB suspension and a conventional silver plate electrode (Fig. 1). When applying a total current density of 50 mA/cm^2, the CO current density of 27 mA/cm^2 (Faradaic efficiency, FE = 54 %) reached in the flow-through system is more than 5 times higher than in the Ag/CB suspension system (max. 5 mA/cm^2, FE < 10 %), and more than 10 times higher than on the Ag plate (max. 2 mA/cm^2, equivalent to comparable flow systems in literature). [8] Although both the flow-through and the CB-suspension systems benefit from a larger volume with accessible CO_2, larger electrode surface area (13.5x larger surface area for carbon foam, >100.000x for Ag/CB suspension), and interrupted electrode surfaces that disrupt diffusion boundary layers, the flow-through electrode holds additional advantages over the Ag/CB suspension system. [37,40] Firstly, the flow-through electrode provides a permanent conductive network that continuously spans the entire channel depth. This offers higher electrical conductivity than the dynamic networks in a suspension electrode, which leads to improved volume utilization. [38–40] Secondly, flowing the suspension particles in the Ag/CB suspension system lowers the relative velocity between the electrode and electrolyte, which likely diminishes the positive effect of electrolyte flow. As a result, the flow-through configuration makes the best use of the available CO_2 and the electrolyte flow.

Despite the stable performance during catalysis shown in Fig. 1, we observe that the Ag NP suspension is not stable. Upon flowing the suspension through the flow-through current collector, the foam acts as a filter and captures most of the suspended Ag NPs within 1 min of recirculation. This is evident from the fast loss of grey color in the fresh

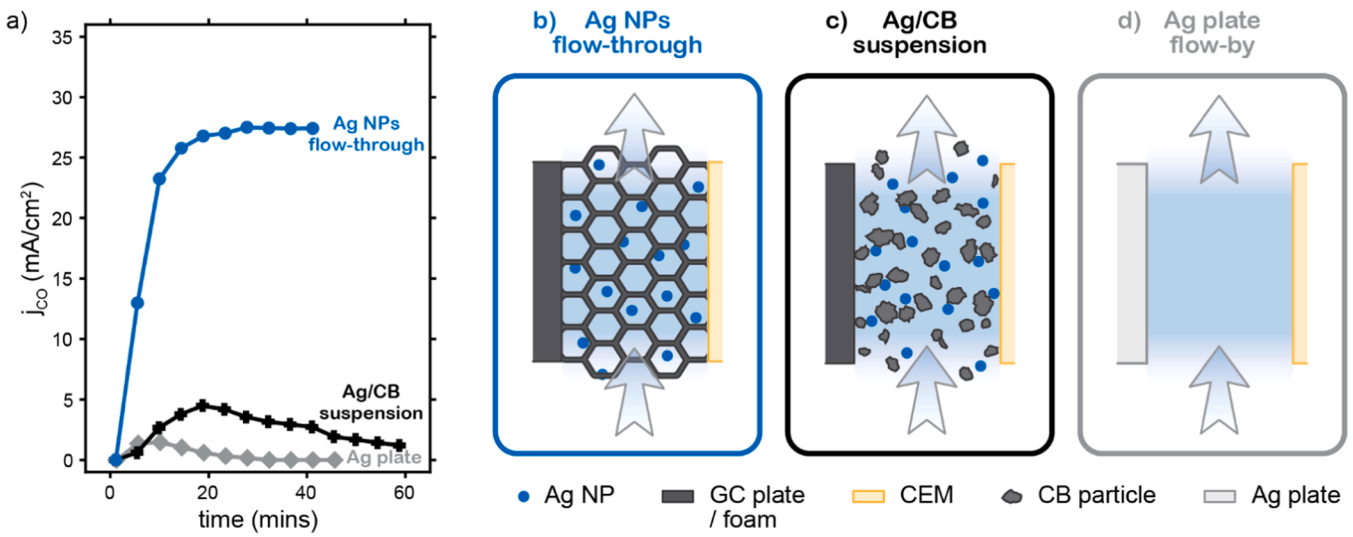

Fig. 1. a) The achieved partial CO current density (j_{CO}) over time for three different flow systems, when operating at a total current density of 50 mA/cm^2. The cathode and anode were both fed with 0.5 M $KHCO_3$, saturated with CO_2 at 1 bar, at 80 mL/min. For the case of Ag NPs flow-through (b), the catholyte contains 0.1 wt% Ag NPs. For the case of Ag/CB suspension (c), the catholyte contains 1.25 wt% Ag NPs and 3.75 wt% carbon black. For the case of Ag plate flow-by, no nanoparticles were added. The j_{CO} equilibrates during the first 10 min of reaction due to flushing of the headspace in the electrolyte container. The catalytic suspension combined with an inert flow-through electrode (Ag NPs flow-through) reaches higher j_{CO} with greater stability than the flowed suspension of carbon black (CB) microparticles and silver nanoparticles (Ag NP), and the conventional flow-by system with a silver plate (Ag plate) electrode.

suspension during pumping (Fig. 2a-b), and from the large amount of Ag NPs that are visibly stuck to the foam section facing the channel inlet (Fig. 2c) and on struts inside the foam (Fig. 2d). We hypothesize that severe agglomeration in the first cm of the current collector is preventing the flow-through from performing at its full potential. Based on the color of the electrolyte, the aggregation process happens at a timescale of < 1 min, and therefore occurs before the product gas reaches a stable composition. Hence, the steady state (Ag NPs after 20 min in Fig. 1a) is reached with a significantly smaller catalytic surface area compared to the initially available area of the suspended Ag NPs. We expect that the performance can be enhanced further by preventing particle aggregation caused by strong Van der Waals forces and weakened electrostatic repulsion in the electrolyte. We can use methods from colloid science, such as adding stabilizing agents, to achieve this [44]. Moreover, some surface additives have shown increased selectivity for the CO_2RR, suggested by locally higher availability of CO_2 at the catalytic surface. [45,46]

Incorporating surfactants into the reactive suspensions, either by adding sodium dodecyl sulfate (SDS) or using pre-coated polyvinylpyrrolidone (PVP)-capped NPs, indeed raises the CO current density when operating at 100 mA/cm^2 (Fig. 3b). At 50 mA/cm^2, the SDS- and PVP-stabilized suspensions produce similar CO current densities compared to the bare Ag NP suspension (27 mA/cm^2) (Fig. 3a), within the error margin of the measurements (see Fig. S4 for the standard errors between multiple series).

At a total current density of 100 mA/cm^2, the SDS-stabilized solution is clearly outperforming the other electrolytes (Fig. 3b). The bare Ag suspension shows a decline in performance during the run at 100 mA/cm^2, which occurs even faster and more drastically when PVP-capped Ag NPs are used. We hypothesize that agglomeration at the electrode surface is alleviated by SDS surfactant. In addition, SDS can lend improved CO selectivity by protecting the NP surface from undergoing

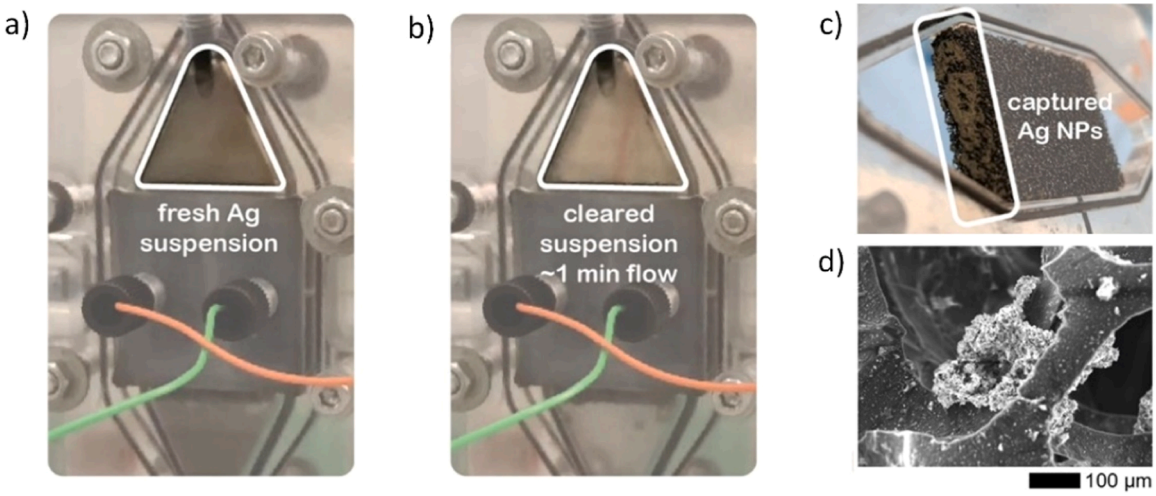

Fig. 2. Pictures of a) the fresh Ag NP suspension inside the flow channel right after starting the pump, and b) the same suspension that clears within one minute of pumping. c) Picture of a used carbon foam with a large quantity of Ag NPs captured and stuck to the side of the foam facing the channel inlet. d) SEM image of used RVC foam with agglomerated Ag NPs on struts of the foam.

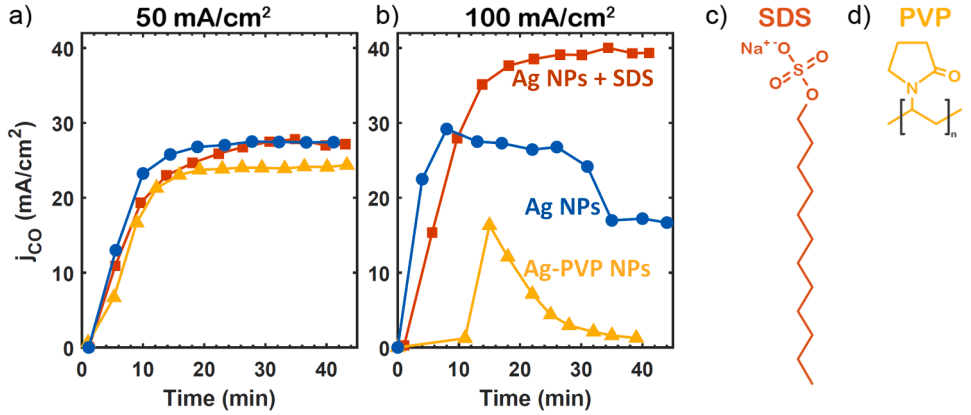

Fig. 3. The achieved CO current densities (j_{CO}) on Ag NP suspensions without surfactant (blue dots), PVP-coated Ag NPs (yellow triangles), and suspensions of Ag NPs with 0.1 wt% of SDS added to the electrolyte (red squares), when applying a) 50 mA/cm^2 and b) 100 mA/cm^2. The molecular structure of SDS and PVP is illustrated in panel c) and d), respectively. j_{CO} is averaged over multiple series; four series for the SDS-case at 50 mA/cm^2, two series for the SDS-case at 100 mA/cm^2, two series for the PVP-case at 50 mA/cm^2, and a single series for the other measurements. Standard deviations are included in Fig. S5.

degradation and morphological changes at highly negative potentials. At strongly negative potentials, PVP will strip off the NP surfaces, initially increasing the availability of active sites and performance, and subsequently degrading the NP surfaces, decreasing the performance. [47] In contrast, the SDS-stabilized suspensions produce a stable CO current density of 40 mA/cm^2 when 100 mA/cm^2 is applied (FE = 40 %), and even withstand 150 mA/cm^2 of applied current density (Fig. S5 in SI), although the achieved CO current density is decreased (25 mA/cm^2, FE = 16 %) compared to 100 mA/cm^2 (Fig. 3b). Although the initial motive for adding surfactants was to repress particle aggregation, surfactants also aid CO_2 reduction by lowering the surface tension and thereby facilitating bubble removal at smaller bubble sizes. [48] This can enhance bubble-induced mass transfer [49], preventing blocking of pores and active sites by large bubbles.

In more detail, SDS is especially interesting as its addition does not prevent the sticking behavior completely, but rather induces potential-dependent repulsion, demonstrated by a cloud of Ag NPs upon applying a negative potential (Fig. S6 in SI). As an anionic surfactant, SDS evidently has a higher repulsion to the negative electrode than the neutral PVP molecules (Fig. 3c-d), which helps to counteract Ag NPs sticking to the foam. We note that previous work on surfactant-supported Ag NP suspension indicated that SDS reduces the agglomerate size [44,50]. Also changing the $KHCO_3$ concentration to 0.1 M, with 0.1 wt% Ag NP + 0.1 wt% SDS, produces similar results as the 0.5 M $KHCO_3$ case (Fig. S8).

Work by Liu et al. [47] indicates that steric hindrance by surfactants can improve particle stability but also hinder CO_2 transfer to the catalytic surface and block active sites. Therefore, we anticipate an optimum in the surfactant-to-particle ratio that lends sufficient stability while preventing the Ag NP surfaces to become too crowded for CO_2 molecules to reach it. Varying the Ag:SDS ratio between 0.1:0 and 0.1:1 (wt%) reveals that the best performance is obtained when both loadings are equal at 0.1 wt% (Fig. 4a). This results in a concentration of 3.5 mM SDS, which is well above the critical micelle concentration (CMC) of SDS in 0.5 M $KHCO_3$. [51] Varying the absolute Ag/SDS concentrations while keeping this ratio fixed at 1 shows that the CO current density is not increased further when raising both concentrations above 0.1 wt% (Fig. 4b). For the highest loading (0.5 wt%), the CO current density even decreases when applying 100 mA/cm^2, while the partial current density is somewhat higher at 50 mA/cm^2, but the differences between these results are close to the error margins. We conclude that the mass transfer (which relates to the catalyst distribution) is limiting rather than the absolute catalyst loading.

In more detail, at 200 mA/cm^2, we also observe a decline in Faradaic efficiency over time (Fig. S5) and high overpotentials at the cathode

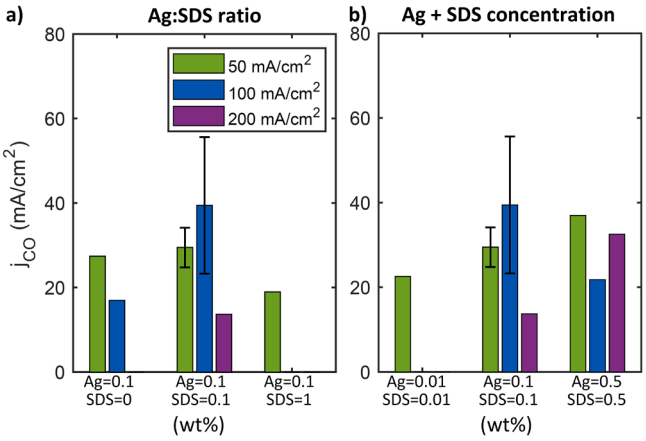

Fig. 4. Resulting CO current density a) at various Ag:SDS ratio's where the Ag concentration is kept constant at 0.1 wt%, and b) at various Ag and SDS concentrations where the Ag:SDS ratio is fixed at 1. The cases with Ag/SDS equal to 0.1/0, 0.1/1, and 0.01/0.01 were not performed at every current density. The 0.1/0.1 case was performed multiple times and the error bars indicate the standard error.

(Fig. 5), caused by the thick cathode foam. We suggest that SDS loses its advantage at these large negative potentials, possibly due to electrochemical decomposition of SDS or too strong repulsion and hence poor charge transfer between the electrode and Ag NPs, causing a decline in CO current density at electrode potentials below −2 V vs RHE. This loss in dispersion functionality at strongly negative potentials is then mitigated at larger concentrations of Ag and SDS (Fig. 4b).

We also note that there is a substantial sample-to-sample variation, both in the voltage applied to the cathode (Fig. 5) as well as in the limiting current density and Faradaic efficiency (Fig. S5 and Fig. S9). Interestingly, we observed consistently better performance when circulating the suspension through the foam electrode before applying the potential, compared saturating the container and applying a current immediately upon filling the flow cell (Fig. 6a). This suggests that having some Ag particles attached to the flow-through electrode promotes CO_2 reduction. This effect implies that the surfactants have mainly the role to improve the spatial distribution and agglomeration size of Ag deposits. SDS would then mitigate the formation of large agglomerates and causes a more evenly distributed coating, thereby increasing the partial current density for CO. Because the coating with Ag NPs is stochastic and causes random flow patterns, further

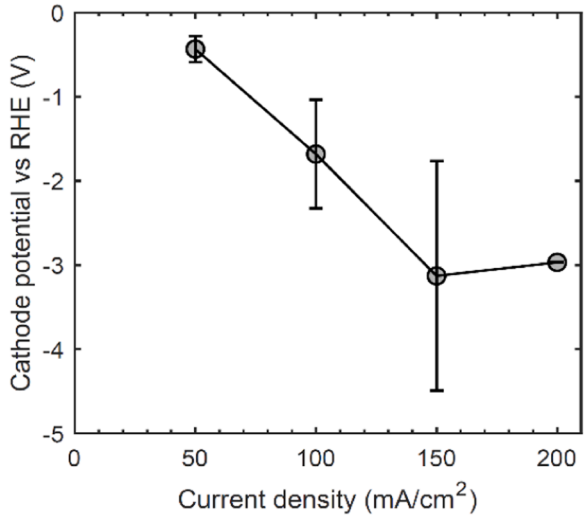

Fig. 5. Cathode potential vs RHE for different current densities, measured for the case of 0.1 wt% Ag + 0.1 wt% SDS. Standard errors are calculated based on potentials independent duplicate and triplicate runs.

complicated by bubble entrapment and repulsion, a large sample-to-sample variation is induced.

To assess different modes for Ag distribution, we also tested silver-coated CB suspension with a flow-through electrode, an Ag NP suspension containing both PVP and SDS, and an Ag NPs + SDS suspension with a flow-through electrode with larger pores (8 pores/cm). None of these configurations performed better than the SDS-stabilized Ag suspensions in combination with the flow-through electrode with standard pore size (24 pores/cm); see Fig. S9. The drastically lower CO current density in the flow-through electrode with larger pores emphasizes the need for microporous electrodes to ensure sufficient Ag particle-electrode interactions.

Finally, to test the stability of this system, we assessed the system with multiple subsequent runs, reaching a total runtime of 250 min without replacing the electrolyte or electrodes (Fig. 6b). Between each runs, we stop the current to saturate the electrolyte with CO_2, ensuring that the rate of dissolution is not limiting and removing all residual CO from the previous section. Apart from the fluctuations in the first minutes of applying each current density, we see no clear degradation over time. Although longer stability remains to be proven in future research, the good performance after 4 h and the stable operation at 100 and 150 mA/cm^2 (where the bare Ag NPs show a decline in Fig. 3b), demonstrates that the SDS is still functional at this timescale and this current density.

As an outlook to a practical application, scaling a flow-through system should not be limited by the dissolved CO_2 capacity; we calculate that only 0.6 % of the available CO_2 in the channel is consumed at the highest partial current densities. Therefore, either the channel can be made longer to raise the portion of utilized CO_2, or the CO current density can be boosted even further (almost 170x, in theory). A structure with pores smaller than the diffusion boundary layer (estimated to be approximately 10 μm for this foam structure [40]) would be ideal. With such intensification, the use of a bipolar membrane could be useful to mitigate the OH^- accumulation, which would merge our concept of surfactant-assisted suspensions in flow-through electrodes with the route of bipolar membrane-based bicarbonate conversion. [52–55]

Comparing flow-through electrodes in this work to other CO_2 electrolyzer concepts, the CO_2-to-CO current density is lower than for gas-fed CO_2 electrolyzers (> 200 mA/cm^2) [12–14], but outperforming simple planar electrodes in aqueous CO_2 electrolysis by an order of magnitude [9]. That brings these flow-through electrodes in the same range as BPM-based bicarbonate conversion [52–55], high-pressure CO_2 conversion [9], or pressure-pulsed CO_2 conversion [56]. This indicates that mass transfer limitations can be alleviated, but that individual concepts do not yet reach the industrial requirements for current density and Faradaic efficiency. Nevertheless, given the room for improvement, and possibilities to combine strategies for aqueous CO_2 conversion, fully aqueous CO_2 conversion might reach the industrial needs for intensified CO_2 electrolysis.

4. Conclusions

Our results show that, for fully aqueous-fed CO_2 electrolyzers, a flow-through electrode in combination with surfactants can significantly improve the CO current density compared to a flow-by system. We obtain partial current densities for CO_2 to CO conversion of 40 mA/cm^2 using a suspension of Ag NPs + SDS flowing through a carbon foam electrode, against 2 mA/cm^2 for a Ag flow-by configuration and 5 mA/cm^2 for a carbon black suspension electrode. The flow-through electrodes benefit both from the larger surface area and thin (interrupted) boundary layers, while still providing good electric conductivity in the

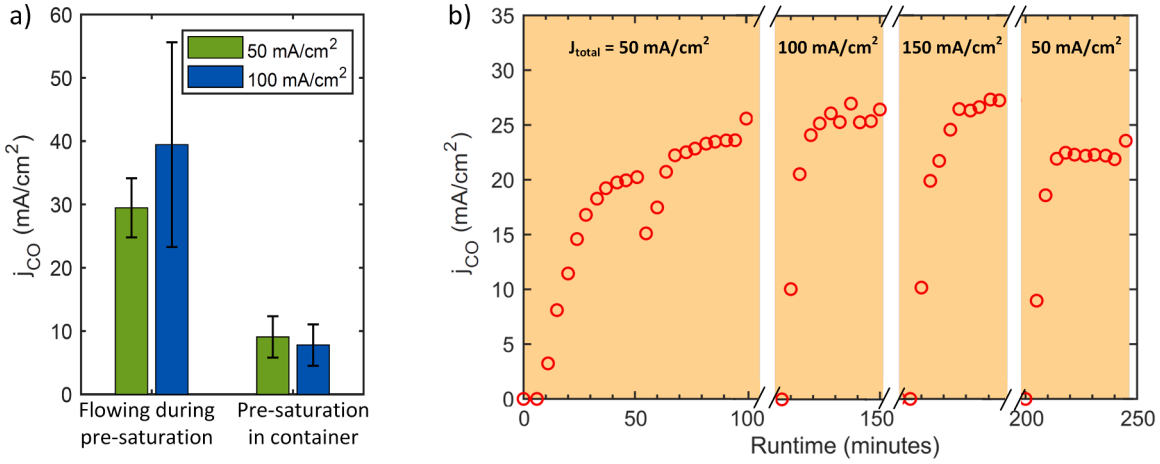

Fig. 6. a) CO current density (values after 45 min, averaged over multiple runs, with standard error) at 50 and 100 mA/cm^2 total current density, for cases where the solution was flowing through the electrochemical cell during pre-saturating with CO_2, and for cases where the solution was pre-saturated in the container only. b) CO current density over time, for series running at 50, 100, 150 and 50 mA/cm^2 without replacing the solution or electrodes, for a total time of 4 h. The j_{CO} dips every 45 min because the solution was purged with CO_2 in between, to remove all residual CO from the previous section. Both cases used a 0.1 wt% Ag NPs suspension + 0.1 wt% SDS.

foam structure. Even though the partial current densities in this aqueous flow-through system are modest compared to gas-fed CO_2 electrolyzers, the strategy of a flow-through electrolyzer is effective to enhance mass transfer. Surfactants are crucial to 1) allow an even distribution of Ag NPs with fewer aggregates and thus more catalytically active surface area, and 2) improve removal of smaller bubbles which enhances bubble-induced mass transfer and prevents large bubbles from blocking pores and active sites. Ultimately, we have shown that a smart electrode design can enhance the CO current density in aqueous electrolyzers considerably, offering an alternative to gas-fed systems as a pathway towards intensifying CO_2 electrolysis.

Funding sources

This project has received funding from the European Research Council (ERC) under the European Union's Horizon 2020 research and innovation programme (Grant agreement No 852115). This work reflects the authors' view and the ERC Executive Agency is not responsible for any use resulting from the information it contains.

Author Contributions

All authors have given approval to the final version of the manuscript. N.E.G. and M.K. performed data curation, methodology, investigation and formal analysis. N.E.G. and D.A.V. performed conceptualization, writing of the original draft and visualization. D.A.V. performed supervision and funding acquisition. J.T.P. performed writing (review and editing) and supervision.

Associated content

The Supporting Information contains: additional information on the methods, flow cell, and setup; (microscopy) images of aggregation in the foam; additional experimental results and observations.

The relevant data is available in the Zenodo repository at 10.5281/zenodo.12750738.

CRediT authorship contribution statement

David A. Vermaas: Writing – original draft, Visualization, Supervision, Funding acquisition, Conceptualization. **Johan T. Padding:** Writing – review & editing, Supervision. **Mohammed A. Khan:** Writing – review & editing, Methodology, Investigation, Formal analysis, Data curation. **Nathalie E.G. Ligthart:** Writing – original draft, Visualization, Methodology, Investigation, Formal analysis, Data curation, Conceptualization.

Declaration of Competing Interest

The authors declare that they have no known competing financial interests or personal relationships that could have appeared to influence the work reported in this paper.

Appendix A. Supporting information

Supplementary data associated with this article can be found in the online version at doi:10.1016/j.jcou.2025.103248.

Data availability

The data is publicly available at ZENODO, and the link is available in the manuscript

References

[1] P. De Luna, et al., What would it take for renewably powered electrosynthesis to displace petrochemical processes? Science 364 (6438) (2019) eaav3506.
[2] H. Geoffrey, N. Marcus, Glasgow climate pact: a step on the way towards a lower carbon dioxide world, in: Proceedings of the Institution of Civil Engineers - Civil Engineering, 175, 2022, 8-8.
[3] P. Gabrielli, M. Gazzani, M. Mazzotti, The role of carbon capture and utilization, carbon capture and storage, and biomass to enable a Net-Zero-CO2 emissions chemical industry, Ind. Eng. Chem. Res. 59 (15) (2020) 7033–7045.
[4] M. Jouny, W. Luc, F. Jiao, General techno-economic analysis of CO2 electrolysis systems, Ind. Eng. Chem. Res. 57 (6) (2018) 2165–2177.
[5] T. Hatsukade, et al., Insights into the electrocatalytic reduction of CO 2 on metallic silver surfaces, Phys. Chem. Chem. Phys. 16 (27) (2014) 13814–13819.
[6] Y. Hori, Electrochemical CO2 reduction on metal electrodes, in: C.G. Vayenas, R. E. White, M.E. Gamboa-Aldeco (Eds.), in Modern aspects of electrochemistry, Springer, 2008, pp. 89–189.
[7] M. Ma, K. Djanashvili, W.A. Smith, Selective electrochemical reduction of CO2 to CO on CuO-derived cu nanowires, Phys. Chem. Chem. Phys. 17 (32) (2015) 20861–20867.
[8] L.M. Baumgartner, et al., Direct imaging of local ph reveals bubble-induced mixing in a CO2 electrolyzer, ACS Sustain. Chem. Eng. 11 (28) (2023) 10430–10440.
[9] M.-Y. Lee, et al., Current achievements and the future direction of electrochemical CO2 reduction: a short review, Crit. Rev. Environ. Sci. Technol. 50 (8) (2020) 769–815.
[10] S. Liang, et al., Electrolytic cell design for electrochemical CO2 reduction, J. CO2 Util. 35 (2020) 90–105.
[11] D. Salvatore, C.P. Berlinguette, Voltage matters when reducing CO2 in an electrochemical flow cell, ACS Energy Lett. 5 (1) (2020) 215–220.
[12] M.G. Kibria, et al., Electrochemical CO2 reduction into chemical feedstocks: from mechanistic electrocatalysis models to system design, Adv. Mater. 31 (31) (2019) 1807166.
[13] R.I. Masel, et al., An industrial perspective on catalysts for low-temperature CO2 electrolysis, Nat. Nanotechnol. 16 (2) (2021) 118–128.
[14] S. Verma, et al., A Gross-Margin model for defining technoeconomic benchmarks in the electroreduction of CO2, ChemSusChem 9 (15) (2016) 1972–1979.
[15] L.M. Baumgartner, et al., Narrow pressure stability window of gas diffusion electrodes limits the Scale-Up of CO2 electrolyzers, ACS Sustain. Chem. Eng. 10 (14) (2022) 4683–4693.
[16] B. De Mot, et al., Direct water injection in catholyte-free zero-gap carbon dioxide electrolyzers, ChemElectroChem 7 (18) (2020) 3839–3843.
[17] K.V. Petrov, et al., Anion-exchange membranes with internal microchannels for water control in CO2 electrolysis, Sustain. Energy Fuels 6 (22) (2022) 5077–5088.
[18] K. Yang, et al., Role of the Carbon-Based gas diffusion layer on flooding in a gas diffusion electrode cell for electrochemical CO2 reduction, ACS Energy Lett. 6 (1) (2021) 33–40.
[19] E.R. Cofell, et al., Investigation of Electrolyte-Dependent carbonate formation on gas diffusion electrodes for CO2 electrolysis, ACS Appl. Mater. Interfaces 13 (13) (2021) 15132–15142.
[20] H. Rabiee, et al., Gas diffusion electrodes (GDEs) for electrochemical reduction of carbon dioxide, carbon monoxide, and dinitrogen to value-added products: a review, Energy Environ. Sci. 14 (4) (2021) 1959–2008.
[21] J. Lee, et al., Electrochemical CO2 reduction using alkaline membrane electrode assembly on various metal electrodes, J. CO2 Util. 31 (2019) 244–250.
[22] H.M. Pelzer, et al., Scaling and heating will drive low-temperature CO2 electrolysers to operate at higher temperatures, Nat. Energy 10 (5) (2025) 549–556.
[23] J.-W. Hurkmans, et al., Heating dictates the scalability of CO2 electrolyzer types, EES Catal. 3 (2025) 305–317.
[24] N.E. Ligthart, et al., 20-Fold increased limiting currents in oxygen reduction with Cu-tmpa by replacing flow-by with flow-through electrodes, ACS Sustain. Chem. Eng. 12 (34) (2024) 12909–12918.
[25] G. Wen, et al., Continuous CO2 electrolysis using a CO2 exsolution-induced flow cell, Nat. Energy 7 (10) (2022) 978–988.
[26] V. Vedharathinam, et al., Using a 3D porous Flow-Through electrode geometry for High-Rate electrochemical reduction of CO2 to CO in ionic liquid, ACS Catal. 9 (12) (2019) 10605–10611.
[27] M.I. Gillespie, F. van der Merwe, R.J. Kriek, Performance evaluation of a membraneless divergent electrode-flow-through (DEFT) alkaline electrolyser based on optimisation of electrolytic flow and electrode gap, J. Power Sources 293 (0) (2015) 228–235.
[28] F. Yang, et al., Alkaline water electrolysis at 25 a cm−2 with a microfibrous Flow-through electrode, Adv. Energy Mater. 10 (25) (2020) 2001174.
[29] F.C. Walsh, et al., The continued development of reticulated vitreous carbon as a versatile electrode material: structure, properties and applications, Electrochim. Acta 215 (2016) 566–591.
[30] A. Rommerskirchen, et al., Unraveling charge transport in carbon flow-electrodes: performance prediction for desalination applications, Carbon 145 (2019) 507–520.
[31] N.J. Matteucci, et al., Toward electrochemical design principles of redox-mediated flow batteries, Curr. Opin. Electrochem. 42 (2023) 101380.
[32] F. Soavi, et al., Semi-solid lithium/oxygen flow battery: an emerging, high-energy technology, Curr. Opin. Chem. Eng. 37 (2022) 100835.
[33] W. Zhang, et al., Selection and optimization of carbon-based electrode materials for flow-electrode capacitive deionization, Sep. Purif. Technol. 315 (2023) 123649.
[34] J. Ma, C. Zhai, F. Yu, Review of flow electrode capacitive deionization technology: research progress and future challenges, Desalination 564 (2023) 116701.

[35] A. Deeke, et al., Fluidized capacitive bioanode as a novel reactor concept for the microbial fuel cell, Environ. Sci. Technol. 49 (3) (2015) 1929–1935.
[36] C. Borsje, et al., Making the best use of capacitive current: comparison between fixed and moving granular bioanodes, J. Power Sources 489 (2021) 229453.
[37] N.E.G. Ligthart, et al., Practical potential of suspension electrodes for enhanced limiting currents in electrochemical CO2 reduction, Energy Adv. 3 (4) (2024) 841–853.
[38] H. Chen, et al., Single-component slurry based lithium-ion flow battery with 3D current collectors, J. Power Sources 485 (2021) 229319.
[39] X. Zhang, et al., Flow-electrode capacitive deionization utilizing three-dimensional foam current collector for real seawater desalination, Water Res. 220 (2022) 118642.
[40] N.E.G. Ligthart, et al., 20-fold increased limiting currents in oxygen reduction with Cu-tmpa by replacing flow-by with flow-through electrodes, ACS Sustain. Chem. Eng. 12 (34) (2024) 12909–12918.
[41] M.E. Suss, et al., Membraneless flow battery leveraging flow-through heterogeneous porous media for improved power density and reduced crossover, RSC Adv. 6 (102) (2016) 100209–100213.
[42] N.M. Delgado, et al., Flow-Through design for enhanced redox flow battery performance, J. Electrochem. Soc. 169 (2) (2022) 020532.
[43] H. Rajaei, A. Rajora, J.W. Haverkort, Design of membraneless gas-evolving flow-through porous electrodes, J. Power Sources 491 (2021) 229364.
[44] X. Li, J.J. Lenhart, H.W. Walker, Aggregation kinetics and dissolution of coated silver nanoparticles, Langmuir 28 (2) (2012) 1095–1104.
[45] Y. Kuang, et al., Engineering interfacial molecular interactions on ag hollow fibre gas diffusion electrodes for high efficiency in CO2 conversion to CO, Chem. A Eur. J. 30 (72) (2024) e202403251.
[46] A.K. Buckley, et al., Approaching 100% selectivity at low potential on ag for electrochemical CO2 reduction to CO using a surface additive, ACS Catal. 11 (15) (2021) 9034–9042.
[47] M. Liu, et al., The capping agent is the key: structural alterations of ag NPs during CO2 electrolysis probed in a zero-gap gas-flow configuration, J. Catal. 404 (2021) 371–382.
[48] N. Kumar, M.Q. Raza, R. Raj, Surfactant aided bubble departure during pool boiling, Int. J. Therm. Sci. 131 (2018) 105–113.
[49] T. Burdyny, et al., Nanomorphology-Enhanced Gas-Evolution intensifies CO2 reduction electrochemistry, ACS Sustain. Chem. Eng. 5 (5) (2017) 4031–4040.
[50] V. Shah, et al., Molecular insights into sodium dodecyl sulphate mediated control of size for silver nanoparticles, J. Mol. Liq. 273 (2019) 222–230.
[51] E. Dutkiewicz, A. Jakubowska, Effect of electrolytes on the physicochemical behaviour of sodium dodecyl sulphate micelles, Colloid Polym. Sci. 280 (11) (2002) 1009–1014.
[52] T. Li, et al., Conversion of bicarbonate to formate in an electrochemical flow reactor, ACS Energy Lett. 5 (8) (2020) 2624–2630.
[53] A.J. Welch, et al., Bicarbonate or carbonate processes for coupling carbon dioxide capture and electrochemical conversion, ACS Energy Lett. 5 (3) (2020) 940–945.
[54] H. Song, et al., Integrated carbon capture and CO production from bicarbonates through bipolar membrane electrolysis, Energy Environ. Sci. 17 (10) (2024) 3570–3579.
[55] H. Song, et al., Ethylene production from carbonate using a bipolar membrane electrolysis system, ACS Appl. Energy Mater. 7 (3) (2024) 1224–1233.
[56] J. Bleeker, et al., Pressure-pulsed flow triples mass transport in aqueous CO2 electrolysis, Chem. Catalysis 0 (2025) 101547.